




Article

Excellent Energy Storage Performance in $\text{Bi}(\text{Fe}_{0.93}\text{Mn}_{0.05}\text{Ti}_{0.02})\text{O}_3$ Modified $\text{CaBi}_4\text{Ti}_4\text{O}_{15}$ Thin Film by Adjusting Annealing Temperature

Tong Liu ^{1,2,†}, Wenwen Wang ^{1,†}, Jin Qian ¹, Qiqi Li ¹, Mengjia Fan ¹, Changhong Yang ^{1,*} , Shifeng Huang ¹ and Lingchao Lu ¹

¹ Shandong Provincial Key Laboratory of Preparation and Measurement of Building Materials, University of Jinan, Jinan 250022, China; shandongmems@163.com (T.L.); wangwenwen_0717@163.com (W.W.); j28_qian@163.com (J.Q.); q1635376692@163.com (Q.L.); fan15176103198@163.com (M.F.); mse_huangsf@ujn.edu.cn (S.H.); mse_lulc@ujn.edu.cn (L.L.)

² MEMS Institute of Zibo National High-Tech Development Zone, Zibo 255000, China

* Correspondence: mse_yangch@ujn.edu.cn

† These authors contributed equally to this work.

Abstract: Dielectric capacitors with ultrahigh power density are highly desired in modern electrical and electronic systems. However, their comprehensive performances still need to be further improved for application, such as recoverable energy storage density, efficiency and temperature stability. In this work, new lead-free bismuth layer-structured ferroelectric thin films of $\text{CaBi}_4\text{Ti}_4\text{O}_{15}$ - $\text{Bi}(\text{Fe}_{0.93}\text{Mn}_{0.05}\text{Ti}_{0.02})\text{O}_3$ (CBTi-BFO) were prepared via chemical solution deposition. The CBTi-BFO film has a small crystallization temperature window and exhibits a polycrystalline bismuth layered structure with no secondary phases at annealing temperatures of 500–550 °C. The effects of annealing temperature on the energy storage performances of a series of thin films were investigated. The lower the annealing temperature of CBTi-BFO, the smaller the carrier concentration and the fewer defects, resulting in a higher intrinsic breakdown field strength of the corresponding film. Especially, the CBTi-BFO film annealed at 500 °C shows a high recoverable energy density of 82.8 J·cm⁻³ and efficiency of 78.3%, which can be attributed to the very slim hysteresis loop and a relatively high electric breakdown strength. Meanwhile, the optimized CBTi-BFO film capacitor exhibits superior fatigue endurance after 10⁷ charge–discharge cycles, a preeminent thermal stability up to 200 °C, and an outstanding frequency stability in the range of 500 Hz–20 kHz. All these excellent performances indicate that the CBTi-BFO film can be used in high energy density storage applications.

Keywords: CBTi-BFO; fine grain; electric breakdown strength; recoverable energy storage



Citation: Liu, T.; Wang, W.; Qian, J.; Li, Q.; Fan, M.; Yang, C.; Huang, S.; Lu, L. Excellent Energy Storage Performance in $\text{Bi}(\text{Fe}_{0.93}\text{Mn}_{0.05}\text{Ti}_{0.02})\text{O}_3$ Modified $\text{CaBi}_4\text{Ti}_4\text{O}_{15}$ Thin Film by Adjusting Annealing Temperature. *Nanomaterials* **2022**, *12*, 730. <https://doi.org/10.3390/nano12050730>

Academic Editors: Dong-Joo Kim and Alain Pignolet

Received: 29 January 2022

Accepted: 18 February 2022

Published: 22 February 2022

Publisher's Note: MDPI stays neutral with regard to jurisdictional claims in published maps and institutional affiliations.



Copyright: © 2022 by the authors. Licensee MDPI, Basel, Switzerland. This article is an open access article distributed under the terms and conditions of the Creative Commons Attribution (CC BY) license (<https://creativecommons.org/licenses/by/4.0/>).

1. Introduction

At present, energy and environmental issues are the focus of social attention. The vigorous development of green and clean energy (such as wind and solar energy) is one of the future trends. The instability and intermittency of green energy put forward higher requirements for energy storage technology [1–5]. Dielectric capacitors typically display ultrafast charge–discharge rates and long life-time, temperature/frequency stability, fatigue resistance, which play key roles in various modern electrical and electronic systems, such as hybrid electric vehicle, aircraft and military [6–9]. Film capacitors offer a smaller size and higher energy storage density, making them easier to integrate into circuits than other devices such as ceramic capacitors [10]. Currently, most commercial dielectrics are mainly made of organic polymers, such as biaxially oriented polypropylene (BOPP), which have been widely used as the dielectric layer in power inverter capacitor systems, making the storage system bulky due to the low energy density (<5 J·cm³). Furthermore, the operating temperature of BOPP cannot be higher than 80 °C, which increases the difficulty of structure

design due to the need for an extra cooling system [11,12]. By contrast, inorganic dielectric film capacitors have the advantages of relatively high energy densities, better thermal stability in wider operating temperature ranges, and long-term endurance. Among this, inorganic ferroelectric film capacitors (TFFCs) are considered as good candidates for energy storage due to their large polarization and high temperature resistance [13,14]. However, low energy storage density and efficiency limit its further development in energy storage applications; thus, further improvements are needed.

For film capacitors, two important energy storage parameters, the recoverable energy storage density (W_{rec}) and energy storage efficiency (η), can be calculated from the measured hysteresis loops adopting the following equations [15,16]:

$$W_{\text{rec}} = \int_{P_r}^{P_m} E dP \quad (1)$$

$$W_t = \int_0^{P_m} E dP \quad (2)$$

$$\eta = \frac{W_{\text{rec}}}{W_t} \times 100\% \quad (3)$$

where E , W_t , P_m and P_r are the applied electric field, total energy storage density, the maximum polarization and remanent polarization during the discharge process, respectively. Therefore, W_{rec} can be improved by increasing the difference between P_m and P_r , and the electric breakdown strength (E_b). It is well known that the E_b of dielectric materials is mainly contingent on its microstructure, such as grain size and degree of densification. Therefore, increasing E_b by reducing grain size is an effective way to improve energy storage performance [17]. Wang et al. sort out the relationship between grain size and electric breakdown strength, confirming the optimization effect of energy storage via grain size-engineering [6]. As is well known, the annealing temperature has an immense impact on the quality of films prepared by chemical solution deposition (CSD). For instance, Wang et al. unveil a large value of W_{rec} up to $91.3 \text{ J}\cdot\text{cm}^{-3}$ at $4993 \text{ kV}\cdot\text{cm}^{-1}$ for $\text{Pb}_{0.88}\text{Ca}_{0.12}\text{ZrO}_3$ (PCZ) antiferroelectric thin films by designing a nanocrystalline structure of the pyrochlore phase by optimizing the annealing temperature to $550 \text{ }^\circ\text{C}$ [18]. However, the negative effect caused by the application of lead-containing dielectrics to human health and environmental sustainability cannot be ignored, and the exploration of lead-free energy storage materials is raised in the agenda. For example, Zuo et al. investigate that a high W_{rec} of $8.12 \text{ J}\cdot\text{cm}^{-3}$ and a great η of $\sim 90\%$ are obtained simultaneously in BiFeO_3 - BaTiO_3 - NaNbO_3 ceramics, which can be attributed to the significantly enhanced E_b of BiFeO_3 -based ternary solid solutions originating from the increased resistivity and refined grain size [19].

Bismuth layer-structured ferroelectric (BLSF) compounds, such as $\text{SrBi}_2\text{Nb}_2\text{O}_9$ (SBN), $\text{SrBi}_2\text{Ta}_2\text{O}_9$ (SBT), $\text{Bi}_4\text{Ti}_3\text{O}_{12}$ (BIT), $\text{CaBi}_4\text{Ti}_4\text{O}_{15}$ (CBTi), belong to a large category of ferroelectric materials [13,20–22]. They have the advantages of excellent anti-fatigue property, large dielectric constant and small dielectric loss, high resistivity and low leakage current density, high ferroelectric Curie transition temperature, and so on [23–26]. Those traits show a good application prospect in the field of dielectric energy storage, but there is little research on BLSF compounds in this field [27,28]. This is mainly due to their intrinsic shortcomings, namely, relatively low polarization and high coercive field, which lead to lower energy density and higher losses in energy storage applications [29]. Recently, Pan et al. presented a composition modification method in ferroelectric Aurivillius $\text{Bi}_{3.25}\text{La}_{0.75}\text{Ti}_3\text{O}_{12}$ by introducing BiFeO_3 to increase the polarization value and optimize hysteresis loops, in which W_{rec} ($113 \text{ J}\cdot\text{cm}^{-3}$) and η (80.4%) are observed. Yang et al. prepared a series of 0.6BaTiO_3 - $0.4\text{Bi}_{3.25}\text{La}_{0.75}\text{Ti}_3\text{O}_{12}$ thin films, and the modified thin film also shows higher dielectric breakdown strength and polarization. CBTi is also a representative BLSF compound, which exhibits distinct advantages including being lead-free and fatigue-free. Meanwhile, it possesses a high Curie point of about $790 \text{ }^\circ\text{C}$ to be used in relatively high temperature applications [30]. However, it also faces troubles of low spontaneous polarization.

In this work, we select $\text{Bi}(\text{Fe}_{0.93}\text{Mn}_{0.05}\text{Ti}_{0.02})\text{O}_3$ introduced into CBTi, namely, CBTi-BFO, to reduce leakage current and enhance breakdown field strength. In order to further optimize the energy storage performance of CBTi-BFO thin films, the effect of annealing temperature on their energy storage capacity has been studied in detail. We found that the microstructures of the CBTi-BFO thin films can be dominated by adjusting the annealing temperature. The CBTi-BFO film annealing at 500 °C possesses an excellent W_{rec} of $82.8 \text{ J}\cdot\text{cm}^{-3}$ and η of 78.3%, simultaneously, due to the obviously enhanced E_b of $3596 \text{ kV}\cdot\text{cm}^{-1}$. Meanwhile, the film shows outstanding temperature/frequency stability up to 150 °C and superior fatigue stability after 10^7 switch cycles. The findings overcome the shortcomings of organic thin films in energy storage, including low energy storage density and low application temperature, unveiling an effective way towards high performance lead-free and eco-friendly ferroelectric materials for energy storage applications.

2. Materials and Methods

Fabrication: CBTi-BFO films were synthesized on Pt/Ti/SiO₂/Si substrates by chemical solution deposition. Bismuth nitrate pentahydrate [$\text{Bi}(\text{NO}_3)_3\cdot 5\text{H}_2\text{O}$], calcium nitrate tetrahydrate [$\text{Ca}(\text{NO}_3)_2\cdot 4\text{H}_2\text{O}$], iron nitrate nonahydrate [$\text{Fe}(\text{NO}_3)_3\cdot 9\text{H}_2\text{O}$], manganese acetate tetrahydrate [$\text{C}_4\text{H}_6\text{MnO}_4\cdot 4\text{H}_2\text{O}$] as raw materials were dissolved in ethylene glycol and acetic acid. Here, 10 mol% excess Bi was added to compensate for elements volatilization. After that, the tetrabutyl titanate and acetylacetone were added into the mixed clarified salt solution. The final concentration of the precursor solution was 0.1 M. After 24 h of aging, the precursor solution was spin coated on Pt/TiO₂/SiO₂/Si substrates with a speed of 4000 rpm for 30 s. After that, the as-prepared CBTi-BFO films were pyrolyzed at 350 °C for 120 s and annealed at 450, 500, 550, 600 °C for 10 min in a rapid thermal annealing procedure, respectively. The spin coating and annealing process procedures were duplicated up till the desired thickness of 300~700 nm was obtained. Circular Pt top electrodes, ~200 μm in diameter, were sputtered through a shadow mask on the films for the next electrical measurements.

Characterization and Measurements: The crystalline structure of CBTi-BFO films was characterized by an X-ray diffractometer (XRD) with Cu K α radiation (XRD, D8 ADVANCE, Karlsruhe, Germany). The cross-sectional microstructure and surface morphology were characterized by a field emission scanning electron microscope (FESEM, ZEISS Gemini300, Oberkochen, Germany). The polarization-electric field (*P-E*) loops and insulating characteristic were acquired from a standard ferroelectric tester (aixACCT TF3000, Aachen, Germany). The frequency-dependent dielectric properties and impedance data were measured using impedance analyzer (HP4294A, Agilent, Palo Alto, CA, US). Impedance data were analyzed by a Z-view software. The temperature-dependent electrical performance tests were completed with the help of a temperature-controlled probe station (Linkam-HFS600E-PB2, London, UK).

3. Results

Figure 1 displays the X-ray diffraction (XRD) patterns of the CBTi-BFO films annealing at four different temperatures and standard JCPDS cards of the target phases. From Figure 1a, as the temperature is at a lower value of 450 °C, most of the diffraction peak of Aurivillius phases have not appeared yet or just a bump, indicating that some amorphous phases formed due to insufficient heat energy. Note that the CBTi-BFO films annealed at 500 and 550 °C show the (119) and (200) diffraction peaks accompanied with another peak with low intensity, which are consistent with the reported results of other CBTi films with Aurivillius phase, demonstrating a polycrystalline bismuth layered structure without any second phase [31–33]. As the annealing temperature continued to rise to 600 °C, apart from the Aurivillius phase, two diffraction peaks that do not belong to the characteristic of the bismuth layered ferroelectric appeared near 15° and 30°, which is due to the formation of the pyrochlore phase of Bi₂Ti₂O₇ [34–37]. Generally, the pyrochlore phase can be formed frequently due to the bismuth element volatilize as the annealing temperature increases,

resulting in the ratio of bismuth ions to titanium ions approaching 1:1. As shown in Figure 1b, the diffraction peak of (119) slightly shifts to a large angle with the increase of the annealing temperature, which may be caused by the release of surface residual stress [38,39].

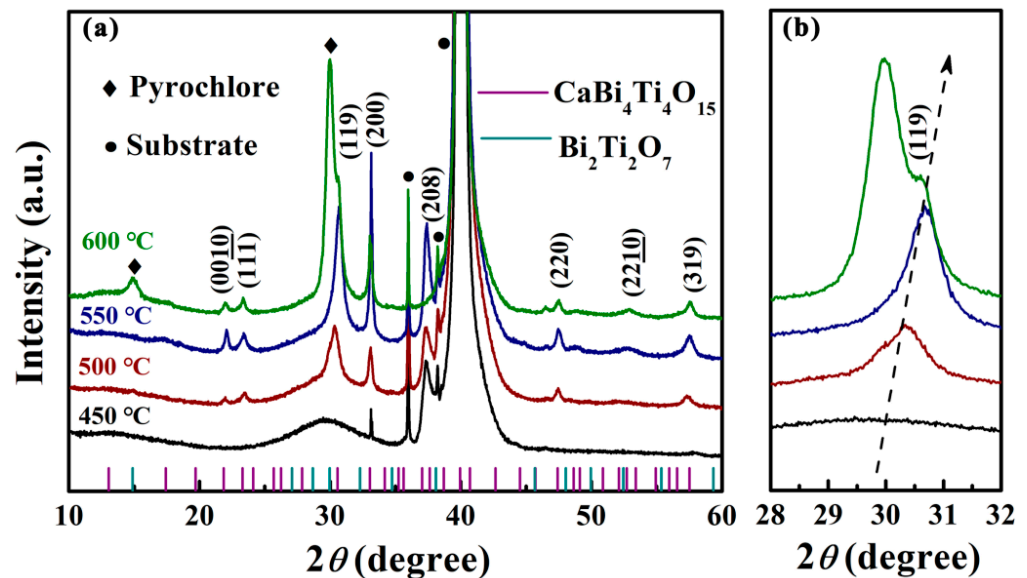


Figure 1. (a) X-ray diffraction (XRD) patterns in the 2θ range of $10\text{--}60^\circ$ of the CBTi-BFO films annealed at various temperatures. (b) Enlarged XRD patterns of the diffraction peaks of 2θ at around 30° .

The SEM images clearly display the surface and the cross-sectional morphologies of the CBTi-BFO thin films annealing at different temperatures. In Figure 2, the inset images reveal that the thickness of all samples is approximately 550 nm. Meanwhile, all CBTi-BFO thin films present compact and pore-free surface, which is favorable to energy storage performance. As shown in Figure 2a, when the film is annealing at 450°C , relatively uniform fine grains can be noticed on the surface. As the temperature rises to 500°C , the grains absorb heat energy and thus, increase uniformly (Figure 2b). In sharp contrast, the CBTi-BFO film annealing at 550°C possesses different grains with a wide range of grain size from ~ 17 to ~ 70 nm in Figure 2c. As the annealing temperature rises up to 600°C , the grain size further increases in the range of ~ 20 to ~ 85 nm (Figure 2d). The phenomenon can be ascribed to: (i) different grain shapes corresponding to different orientations [40]; (ii) an inhomogeneous nucleation and grain-growth at a high annealing temperature [41].

It is well known that thin film with a high dielectric constant (ϵ_r) typically achieves tremendous recoverable energy density and energy efficiency [27,42]. Figure 3a presents the room-temperature frequency dependence of dielectric constant (ϵ_r) and the dissipation factor ($\tan\delta$) of the CBTi-BFO thin films annealing at different temperatures. The ϵ_r value of each film slightly decreases with the frequency raising, and increases obviously with the annealing temperature increasing. The values of ϵ_r for the films annealing at 450 and 500°C have slightly changed with the frequency increases, indicating that the samples annealed at these two temperatures have better frequency stability. Generally, the dielectric properties of ferroelectric film contain the intrinsic and extrinsic contributions, which could be influenced by different factors, such as the grain size, preferred orientation, and so on [43,44]. The reason that in the changes of ϵ_r with increasing annealing temperature may be due to the fact that the increased annealing temperature resulted in the increased grain size and reduced grain boundaries, leading to the enhancement of ϵ_r [27]. Moreover, the dielectric loss ($\tan\delta$) gradually increases with increasing frequency in all samples. Besides, all samples possess smaller loss ($\tan\delta < 0.08$) at 10 kHz.

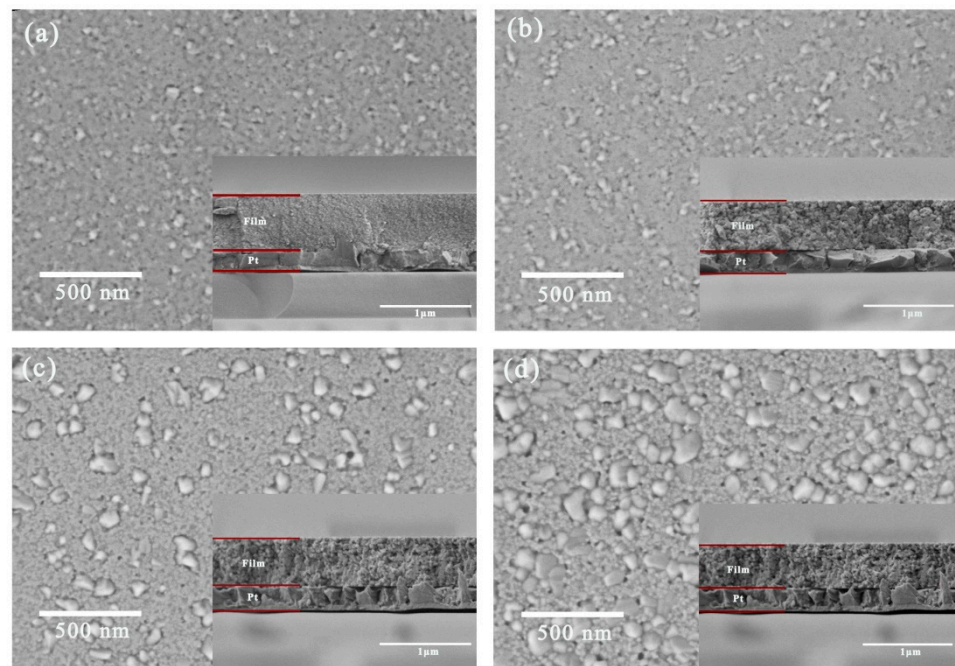


Figure 2. The scanning electron microscopic (SEM) images of the CBTi-BFO thin films annealed at (a) 450 °C, (b) 500 °C, (c) 550 °C and (d) 600 °C, and the inset shows their corresponding cross-sectional micrographs.

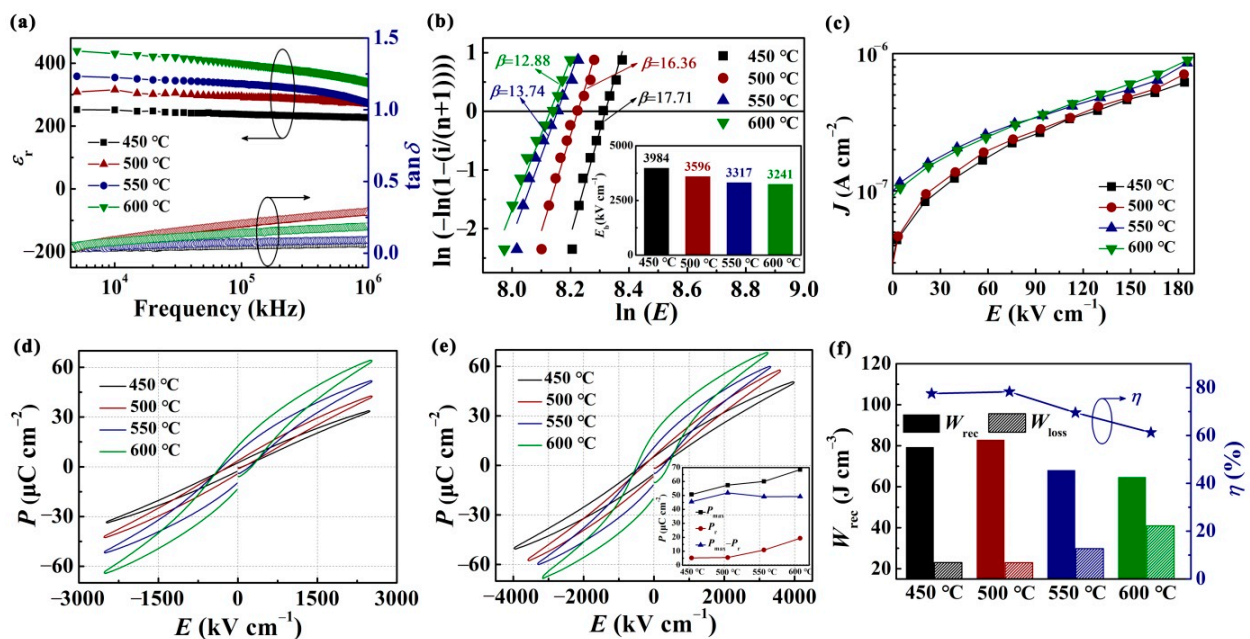


Figure 3. CBTi-BFO films annealed at 450, 500, 550 and 600 °C: (a) Frequency dependence of dielectric properties. (b) Weibull distributions dielectric breakdown strengths. (c) Leakage current density as a function of applied electric field. (d) The bipolar P - E loops at $2500 \text{ kV}\cdot\text{cm}^{-1}$. (e) The bipolar P - E loops around E_b , The inset shows the variation of P_{\max} , P_r , and $P_{\max}-P_r$ as a function of annealing temperature. (f) The variations of W_{rec} , W_{loss} and η values.

Generally, E_b is analyzed by two parameter Weibull statistics, which is closely affected the energy storage performance of dielectric materials [45], as displayed in Figure 3b. Meanwhile, the E_b endurance of four films with different annealing temperatures are

demonstrated in the inset of Figure 3b. The Weibull distribution of E_b can be expressed by the following formulas:

$$X_i = Ln(E_i) \quad (4)$$

$$Y_i = Ln(-Ln(1 - \frac{i}{n+1})) \quad (5)$$

where E_i is the breakdown electric field for each sample, i signifies the number of test samples and n denotes the total number of test samples. Based on the Weibull distribution function, the mean E_b for each film can be obtained from the intersection of the fitted lines with the horizontal axis at $Y_i = 0$. β represents Weibull shape parameter. It can be observed that E_b increases rapidly with the annealing temperature decreasing, as shown in the inset of Figure 3b. The average breakdown strength of the dielectric film increases from $3241 \text{ kV}\cdot\text{cm}^{-1}$ to $3984 \text{ kV}\cdot\text{cm}^{-1}$, with the annealing temperature decrease from 600 to 450 °C. The enhancement of dielectric breakdown strength can be ascribed to the following factor. It is well-known that electric breakdown field strength is inversely proportional to the grain size (G), which can be manifested by the following formula:

$$E_b \propto (G)^{-a} \quad (6)$$

where a is the exponent values, being in the range of 0.2 – 0.4 [6,46]. It can be seen that the dielectric breakdown strength increases with the decreased grain size, which is aligned with the results in Figures 2 and 3b. That is owing to grain boundaries producing depletion regions similar to Schottky barriers located in semiconductor interfaces. Then, the grain boundaries depletion layers establish important barriers for the cross-transport of ionic and electronic charges [47]. Therefore, the E_b for CBTi-BFO film annealing at 450 °C is superior to the films that have higher annealing temperature. The slope parameter β , related to the scatter of E_b data, increases from 12.88 to 17.71 with the annealing temperature decrease from 600 °C to 450 °C, indicating an enhancement in dielectric reliability by annealing temperature decreasing. At the same time, the β of all films based on the linear fitting is higher than 12 , suggestive of all samples possessing high reliability.

Figure 3c represents the leakage current of all films, which are measured by applying 0 – $185 \text{ kV}\cdot\text{cm}^{-1}$ to the electrodes. The CBTi-BFO films annealed at 450 and 500 °C illustrate well insulating properties with leakage current densities $< 7 \times 10^{-7} \text{ A cm}^{-2}$ under an applied electric field of $185 \text{ kV}\cdot\text{cm}^{-1}$. The CBTi-BFO films annealed at 550 and 600 °C exhibit higher leakage currents, which is ascribed to the greater grain size and the simultaneously declined number of the grain boundary.

Presented in Figure 3d are bipolar polarization-electric field (P - E) loops of the CBTi-BFO films annealing at different temperatures applying the electric field of $2500 \text{ kV}\cdot\text{cm}^{-1}$ at frequency of 10 kHz . With the annealing temperature decreasing, a monotonous decrease of polarization (P_{\max}) is observed, from $33 \mu\text{C cm}^{-2}$ of 450 °C to $63 \mu\text{C cm}^{-2}$ of 600 °C.

Figure 3e shows P - E loops of CBTi-BFO films near their respective E_b annealing at different temperatures. It can be seen that the CBTi-BFO thin film annealing at 600 °C presents a practically saturated P - E loop with a remnant polarization P_r of $20 \mu\text{C}/\text{cm}^2$, which is lower than previous reports [32,33], suggesting that the derived CBTi-BFO thin films have somewhat discrepant ferroelectric properties. For the CBTi-BFO thin films annealing at lower temperatures, the obtained P - E hysteresis loops exhibit slim shape, which can be ascribed to the function of lower leakage current and small crystallite size [48–50]. Figure 3f presents the corresponding energy storage parameters of W_{rec} , W_{loss} and η determined from P - E loops about all CBTi-BFO films. The value of W_{rec} and η for the CBTi film annealing at 500 °C, respectively, reaches $82.8 \text{ J}\cdot\text{cm}^{-3}$ and 78.3% due to an integration of remarkable E_b of $3596 \text{ kV}\cdot\text{cm}^{-1}$ and a large polarization disparity of $52.3 \mu\text{C cm}^{-2}$ (inset of Figure 3e). It is well known that the dielectric film can induce outstanding energy performance due to high P_{\max} , low P_r and high electric breakdown strength. The lower annealing temperature leads to more slender electric hysteresis loops and lower W_{loss} . Meanwhile, E_b is enhanced with the decrease of the annealing temperature.

Figure 4a–d show the Nyquist plots of films measured in the frequency range of 100 Hz to 1 MHz at a series of temperatures (225–300 °C). As is known to all, a low-frequency arc means the dielectric response of grain boundaries, while a high-frequency arc means the dielectric response of grains. One semicircular arc is observed for the samples. As the grain boundary dielectric relaxation of the material mainly contributes to the total impedance, only the semi-circular arc corresponding to the grain boundary response is observed. The intercept of impedance semicircular arcs on the Z' -axis can represent the total resistance (R_b) values of the film. Clearly, the value of R_b gradually decreased with the increasing measured temperature in each film, showing a negative temperature characteristic. This phenomenon can be attributed to the fact that the mobility of the space charge becomes easier, and more charge carriers will accumulate at the grain boundaries with the increasing measured temperature, thus resulting in increased electrical conductivity and decreased grain boundary resistance [51,52].

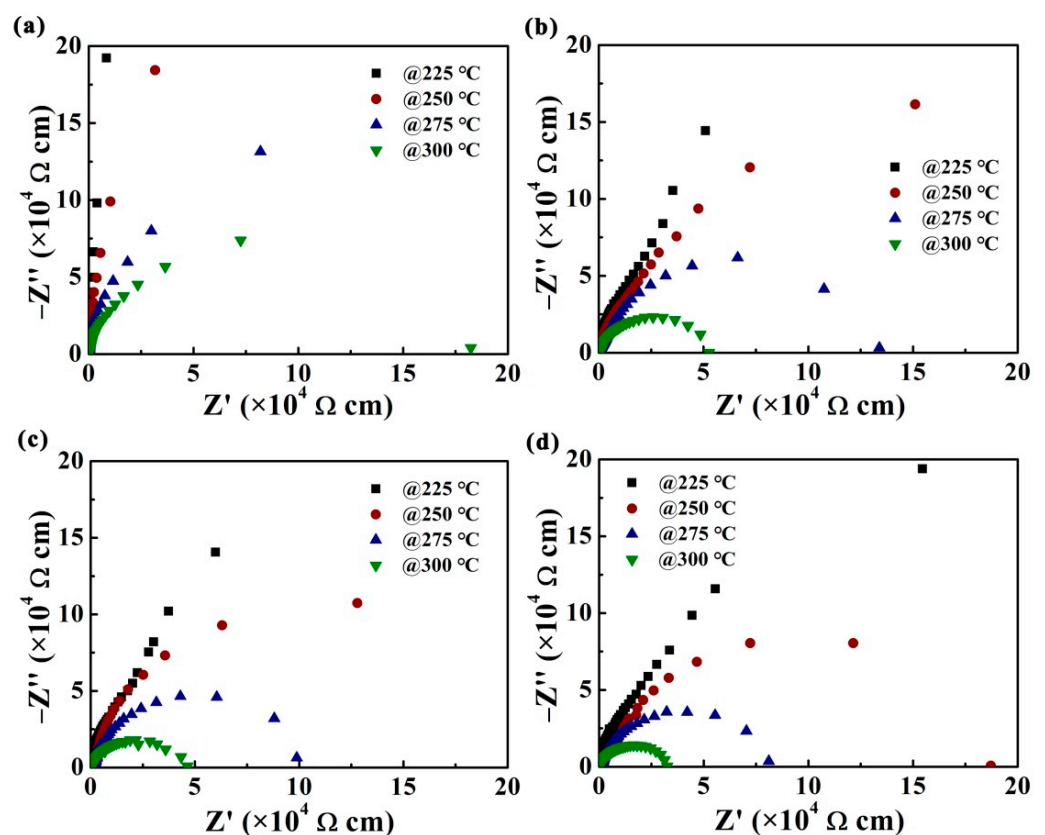


Figure 4. Nyquist diagrams of complex-plane of the CBTi-BFO films with annealing temperature of (a) 450, (b) 500, (c) 550, (d) 600 °C measured at 20 V under four measured temperatures.

In order to compare the impedance differences of the four samples in more detail, we separately take out the impedance diagrams tested at 300 °C and showed them in Figure 5a. It can be seen that R_b of CBTi-BFO films gradually increases with a decreasing annealing temperature, indicating that the charge carrier concentration decreases in low-temperature annealed samples [53].

Generally, the energy required for carriers to cross the energy barrier is called conductive activation energy (E_a), which can be calculated by Arrhenius formula:

$$\sigma = \sigma_0 \exp(-E_a/k_B T) \quad (7)$$

where T , σ_0 , E_a and k_B are the measuring temperature on the Kelvin scale, preexponential factor, activation energy and Boltzmann constant, respectively. The plots of $\ln(\sigma)$ as a function of $1000/T$ for the films and linear fittings are shown in Figure 5b. The activation

energies (E_a) obtained from the slopes of fitting lines for films annealing at 450, 500, 550, 600 °C are estimated to be 1.21, 0.84, 0.68, 0.66 eV, respectively. Generally, the higher value of activation energy means fewer defects exist in the film [54]. Thus, we can deduce that the sample with the lowest annealing temperature has the least defects. Combining the above two points, it can be seen that CBTi-BFO with lowest annealing temperature possesses the smallest charge carrier concentration and fewer defects, which contribute greatly to the observed highest intrinsic breakdown field in this film.

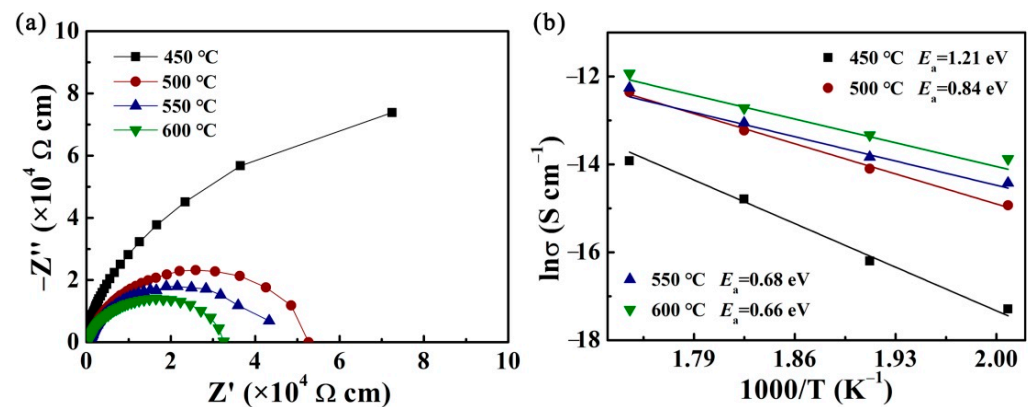


Figure 5. (a) The impedance and fit result of CBTi-BFO films measured at 300 °C. (b) Arrhenius plots of CBTi-BFO films annealing at different temperatures.

For practical application, the requirement of reliability and stability is emphasized, such as under high/low temperature, high/low frequency and long-term working environments. Thus, in view of the CBTi-BFO film annealing at 500 °C possessing large W_{rec} and η among all samples, further investigations are carried out on it under an electric field of $2500 \text{ kV}\cdot\text{cm}^{-1}$. Firstly, the temperature stability of the CBTi-BFO film annealing at 500 °C is measured. The bipolar P - E loops of the film measured from relatively low temperature of $-25 \text{ }^\circ\text{C}$ to ultrahigh temperature of $200 \text{ }^\circ\text{C}$ are displayed in Figure 6a. For the purpose of expressing the variation of polarization more clearly, the unipolar hysteresis loop diagrams' dependence on temperature is drawn in Figure 6d. It can be seen that the P_{max} value varies slightly from 42.62 to $45.89 \text{ } \mu\text{C}\cdot\text{cm}^{-2}$. Correspondingly, W_{rec} values are slightly increased by 2% from 44.88 to $45.84 \text{ J}\cdot\text{cm}^{-3}$ and η is reduced by 6% from 80.04 to 75.19% with temperature increasing, as shown in Figure 6g. The aforesaid energy storage performance of the film shows good temperature stability, which is adequate to meet the demands of applications in extreme environments (capacitors used in underground industrial instruments need to work at temperatures higher than $150 \text{ }^\circ\text{C}$ and the inverter must work at about $140 \text{ }^\circ\text{C}$ in HEV) [55–57]. Besides, frequency dependence of the energy storage behavior is also researched at $2500 \text{ kV}\cdot\text{cm}^{-1}$. Figure 6b, e are the bipolar and unipolar hysteresis loops measured at the frequency range of 500 Hz to 20 kHz, respectively; and the corresponding energy performance W_{rec} and η are shown in Figure 6h. Clearly, the P - E loop can maintain a slim feature and no discernible decline in energy storage performance can be discovered. Even though the frequency rises from 500 Hz to 20 kHz, the W_{rec} and η values slightly drop from 48.71 to $43.80 \text{ J}\cdot\text{cm}^{-3}$ and 83.94 to 77.47% , respectively, indicating that a good frequency stability can be realized. Furthermore, to assess the long-term charging–discharging stability of dielectric capacitors, the fatigue endurance should be investigated. The P - E loops of CBTi-BFO film annealing at 500 °C over 10^7 charge–discharge cycles are exhibited in Figure 6c, f. It can be seen that there is no obvious change in the hysteresis loops. The corresponding W_{rec} and an excellent η present a negligible degradation with 1% and 0.3% as shown in Figure 6i. The observed superior antifatigue feature is closely related to the $(\text{Bi}_2\text{O}_2)^{2+}$ layer in the Aurivillius phase, which has a good insulating effect inhibiting the flow and generation of leakage charges during the repeated polarization process. Thus,

the Aurivillius phase can more effectively suppress the electrical breakdown during the fatigue process and improve the anti-fatigue performance.

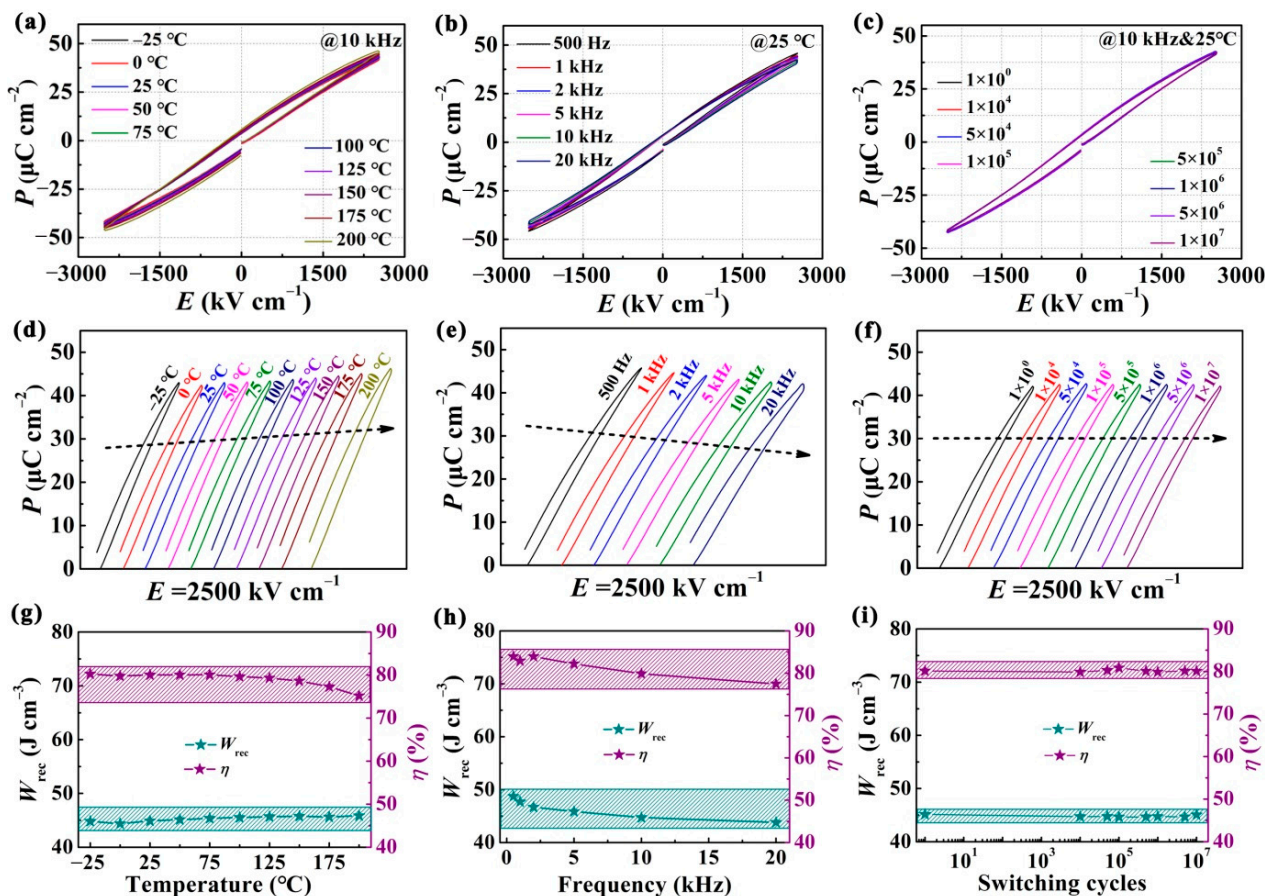


Figure 6. CBTi-BFO thin film annealed at 500 °C: (a–c) bipolar P - E hysteresis loops measured at different temperatures/frequencies/switching cycles; (d–f) unipolar P - E hysteresis loops of CBTi-BFO films at different temperatures/frequencies/switching cycles; (g–i) the changes of W_{rec} and η depending on temperature/frequencies/switching cycles.

Figure 7 summarizes a series of results on the energy storage performance of Aurivillius ferroelectric films [12,13,27,28,58–60]. In this study, the CBTi-BFO thin film annealing at 500 °C possesses a relatively high η (~78%) superior than BaLa_{0.2}Bi_{3.8}Ti₄O₁₅ (BLBT~60%) and Bi_{3.25}La_{0.75}Ti₃O₁₂/BiFeO₃/Bi_{3.25}La_{0.75}Ti₃O₁₂ (BLT/BFO/BLT~74%), but inferior to Ba₂Bi₄Ti₅O₁₈ (BBT~92%), 0.6BaTiO₃-0.4Bi_{3.25}La_{0.75}Ti₄O₁₂ (0.6BT-0.4BLT~84%), CaBi₂Nb₂O₉ (CBNO~82%), Sr₂Bi₄Ti₅O₁₈ (SBT~81%), Bi_{3.25}La_{0.75}Ti₃O₁₂-BiFeO₃ (BLT-BFO~80%). In contrast, its W_{rec} clearly outperforms the surveyed dielectric systems with a high η . That is, the CBTi-BFO thin film annealing at 500 °C has excellent comprehensive properties, namely, a good balance between W_{rec} and η . Meanwhile, the film has a great E_b (~3596 kV·cm⁻¹) at a high level. Taken together, the CBTi-BFO thin film annealing at 500 °C is a good candidate for application in energy storage devices.

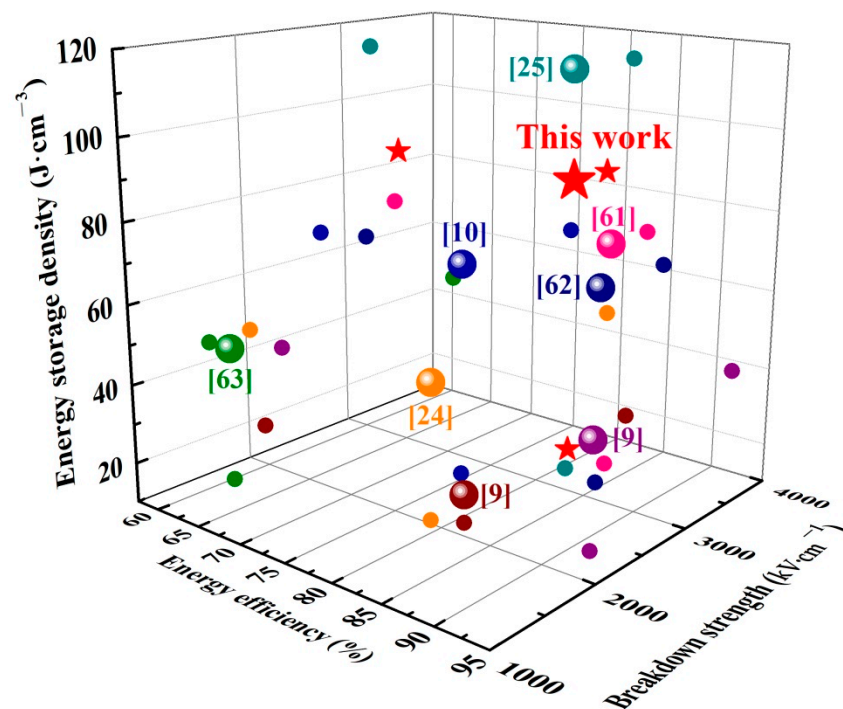


Figure 7. Summary of recently reported the core parameters of E_b , W_{rec} and η for energy storage properties of representative Aurivillius ferroelectrics film [12,13,27,28,58–60].

4. Conclusions

In this work, a series of CBTi-BFO thin films are prepared by chemical solution deposition under different annealing temperatures. We found that by optimizing the microstructures and crystalline structure of films via adjusting the annealing temperature, the electrical properties and energy storage performance can be greatly improved, especially in the film with a relatively lower annealing temperature. In the annealing temperature of 500–550 °C, CBTi-BFO thin films demonstrates a polycrystalline bismuth layered structure without any second phase. The CBTi-BFO with the lowest annealing temperature has the smallest carrier concentration and fewer defects, which greatly contribute to the highest intrinsic breakdown field of this film. Here, ultrahigh energy storage density of W_{rec} ($\sim 82.8 J \cdot cm^{-3}$) and η ($\sim 78.3\%$) are achieved in the CBTi-BFO film that annealed at 500 °C. The excellent energy storage performance can be ascribed to its uniform fine grain size. The film also shows superior thermal stability (from -25 to 200 °C), frequency stability (from 500 Hz to 20 kHz) and fatigue endurance (after 10^7 switching cycles). In a word, annealing temperature plays an important part in performance tuning, which is a vital factor needed to be considered for preparing thin film capacitors with high energy storage characteristics.

Author Contributions: Conceptualization, C.Y., S.H. and L.L.; methodology, C.Y.; investigation, T.L., W.W., J.Q. and Q.L.; resources, C.Y.; data curation, T.L., W.W. and M.F.; writing—original draft preparation, T.L. and W.W.; writing—review and editing, C.Y. and S.H.; supervision, C.Y., S.H. and L.L. All authors have read and agreed to the published version of the manuscript.

Funding: This work was supported by the National Natural Science Foundation of China (Grant Nos. 51972144, and U1806221), the Shandong Provincial Natural Science Foundation (Grant No. ZR2020KA003), the Project of “20 Items of University” of Jinan (Grant Nos. T202009 and T201907), and the Synergetic Innovation Center Research Project (Grant No. WJGTT-XT2), the Introduction Program of Senior Foreign Experts (G2021024003L).

Data Availability Statement: Not applicable.

Conflicts of Interest: The authors declare no conflict of interest.

References

1. Yan, F.; Huang, K.W.; Jiang, T.; Zhou, X.F.; Shi, Y.J.; Ge, G.L.; Shen, B.; Zhai, J.W. Significantly enhanced energy storage density and efficiency of BNT-based perovskite ceramics via A-site defect engineering. *Energy Storage Mater.* **2020**, *30*, 392–400. [[CrossRef](#)]
2. Yao, Z.H.; Song, Z.; Hao, H.; Yu, Z.Y.; Cao, M.; Zhang, S.; Lanagan, M.T.; Liu, H.X. Homogeneous/Inhomogeneous-Structured Dielectrics and Their Energy-Storage Performances. *Adv. Mater.* **2017**, *29*, 1601727. [[CrossRef](#)] [[PubMed](#)]
3. Yan, F.; Shi, Y.J.; Zhou, X.F.; Zhu, K.; Shen, B.; Zhai, J.W. Optimization of polarization and electric field of bismuth ferrite-based ceramics for capacitor applications. *Chem. Eng. J.* **2021**, *417*, 127945. [[CrossRef](#)]
4. Silva, J.P.B.; Silva, J.M.B.; Oliveira, M.J.S.; Weingärtner, T.; Sekhar, K.C.; Pereira, M.; Gomes, M.J.M. High-Performance Ferroelectric-Dielectric Multilayered Thin Films for Energy Storage Capacitors. *Adv. Funct. Mater.* **2018**, *29*, 1807196. [[CrossRef](#)]
5. Wang, W.W.; Qian, J.; Geng, C.H.; Fan, M.J.; Yang, C.H.; Lu, L.C.; Cheng, Z.X. Flexible Lead-Free $\text{Ba}_{0.5}\text{Sr}_{0.5}\text{TiO}_3/0.4\text{BiFeO}_3-0.6\text{SrTiO}_3$ Dielectric Film Capacitor with High Energy Storage Performance. *Nanomaterials* **2021**, *11*, 3065. [[CrossRef](#)] [[PubMed](#)]
6. Wang, G.; Lu, Z.L.; Li, Y.; Li, L.H.; Ji, H.F.; Feteira, A.; Zhou, D.; Wang, D.W.; Zhang, S.J.; Reaney, I.M. Electroceramics for High-Energy Density Capacitors: Current Status and Future Perspectives. *Chem. Rev.* **2021**, *121*, 6124–6172. [[CrossRef](#)] [[PubMed](#)]
7. Palneedi, H.; Peddigari, M.; Hwang, G.-T.; Jeong, D.-Y.; Ryu, J. High-Performance Dielectric Ceramic Films for Energy Storage Capacitors: Progress and Outlook. *Adv. Funct. Mater.* **2018**, *28*, 1803665. [[CrossRef](#)]
8. Qian, J.; Han, Y.J.; Yang, C.H.; Lv, P.P.; Zhang, X.F.; Feng, C.; Lin, X.J.; Huang, S.F.; Cheng, X.; Cheng, Z.X. Energy storage performance of flexible NKBT/NKBT-ST multilayer film capacitor by interface engineering. *Nano Energy* **2020**, *74*, 104862. [[CrossRef](#)]
9. Chu, B.J.; Zhou, X.; Ren, K.L.; Neese, B.; Lin, M.; Wang, Q.; Bauer, F.; Zhang, Q.M. A Dielectric Polymer with High Electric Energy Density and Fast Discharge Speed. *Science* **2006**, *313*, 334–336. [[CrossRef](#)]
10. Fan, Z.J.; Li, L.L.; Mei, X.S.; Zhao, F.; Li, H.J.; Zhuo, X.S.; Zhang, X.F.; Lu, Y.; Zhang, L.; Liu, M. Multilayer ceramic film capacitors for high performance energy storage: Progress and outlook. *J. Mater. Chem. A* **2021**, *9*, 946. [[CrossRef](#)]
11. Dang, Z.M. *Dielectric Polymer Materials for High-Density Energy Storage*; William Andrew: Norwich, NY, USA, 2018.
12. Yang, B.B.; Guo, M.Y.; Tang, X.W.; Wei, R.H.; Hu, L.; Yang, J.; Song, W.H.; Dai, J.M.; Lou, X.J.; Zhu, X.B.; et al. Lead-free $\text{A}_2\text{Bi}_4\text{Ti}_5\text{O}_{18}$ thin film capacitors (A = Ba and Sr) with large energy storage density, high efficiency, and excellent thermal stability. *J. Mater. Chem. C* **2019**, *7*, 1888–1895. [[CrossRef](#)]
13. Yang, B.B.; Guo, M.Y.; Jin, L.H.; Tang, X.W.; Wei, R.H.; Hu, L.; Yang, J.; Song, W.H.; Dai, J.M.; Lou, X.J.; et al. Ultrahigh energy storage in lead-free $\text{BiFeO}_3/\text{Bi}_{3.25}\text{La}_{0.75}\text{Ti}_3\text{O}_{12}$ thin film capacitors by solution processing. *Appl. Phys. Lett.* **2018**, *112*, 033904. [[CrossRef](#)]
14. Chen, P.; Chu, B.J. Improvement of dielectric and energy storage properties in $\text{Bi}(\text{Mg}_{1/2}\text{Ti}_{1/2})\text{O}_3$ -modified $(\text{Na}_{1/2}\text{Bi}_{1/2})_{0.92}\text{Ba}_{0.08}\text{TiO}_3$ ceramics. *J. Eur. Ceram. Soc.* **2016**, *36*, 81–88. [[CrossRef](#)]
15. Burn, I.; Smyth, D.M. Energy Storage in Ceramic Dielectrics. *J. Mater. Sci.* **1972**, *7*, 339–343. [[CrossRef](#)]
16. Lv, P.P.; Yang, C.H.; Qian, J.; Wu, H.T.; Huang, S.F.; Cheng, X.; Cheng, Z.X. Flexible Lead-Free Perovskite Oxide Multilayer Film Capacitor Based on $(\text{Na}_{0.8}\text{K}_{0.2})_{0.5}\text{Bi}_{0.5}\text{TiO}_3/\text{Ba}_{0.5}\text{Sr}_{0.5}(\text{Ti}_{0.97}\text{Mn}_{0.03})\text{O}_3$ for High-Performance Dielectric Energy Storage. *Adv. Energy Mater.* **2020**, *10*, 1904229. [[CrossRef](#)]
17. Zhao, L.; Liu, Q.; Gao, J.; Zhang, S.; Li, J.F. Lead-Free Antiferroelectric Silver Niobate Tantalate with High Energy Storage Performance. *Adv. Mater.* **2017**, *29*, 1701824. [[CrossRef](#)]
18. Li, Y.Z.; Lin, J.L.; Bai, Y.; Li, Y.X.; Zhang, Z.D.; Wang, Z.J. Ultrahigh-Energy Storage Properties of $(\text{PbCa})\text{ZrO}_3$ Antiferroelectric Thin Films via Constructing a Pyrochlore Nanocrystalline Structure. *ACS Nano* **2020**, *14*, 6857–6865. [[CrossRef](#)]
19. Qi, H.; Xie, A.; Tian, A.; Zuo, R. Superior Energy-Storage Capacitors with Simultaneously Giant Energy Density and Efficiency Using Nanodomain Engineered $\text{BiFeO}_3\text{-BaTiO}_3\text{-NaNbO}_3$ Lead-Free Bulk Ferroelectrics. *Adv. Energy Mater.* **2020**, *10*, 1903338. [[CrossRef](#)]
20. Kato, K.; Zheng, C.; Finder, J.M.; Dey, S.K. Sol-Gel Route to Ferroelectric Layer-Structured Perovskite $\text{SrBi}_2\text{Ta}_2\text{O}_9$ and $\text{SrBi}_2\text{Nb}_2\text{O}_9$ Thin Films. *J. Am. Ceram. Soc.* **1998**, *81*, 1869–1875. [[CrossRef](#)]
21. Osaka, T.; Sakakibara, A.; Seki, T.; Ono, S.; Koiwa, I.; Hashimoto, A. Phase Transition in Ferroelectric $\text{SrBi}_2\text{Ta}_2\text{O}_9$ Thin Films with Change of Heat-treatment Temperature. *Jpn. J. Appl. Phys.* **1998**, *37*, 597–601. [[CrossRef](#)]
22. Cheng, C.-M.; Chen, K.-H.; Tsai, J.-H.; Wu, C.-L. Solution-based fabrication and electrical properties of $\text{CaBi}_4\text{Ti}_4\text{O}_{15}$ thin films. *Ceram. Int.* **2012**, *38*, S87–S90. [[CrossRef](#)]
23. Dubey, S.; Kurchania, R. Study of dielectric and ferroelectric properties of five-layer Aurivillius oxides: $\text{A}_2\text{Bi}_4\text{Ti}_5\text{O}_{18}$ (A = Ba, Pb and Sr) synthesized by solution combustion route. *Bull. Mater. Sci.* **2015**, *38*, 1881–1889. [[CrossRef](#)]
24. Park, B.H.; Kang, B.S.; Bu, S.D.; Noh, T.W.; Lee, J.; Jo, W. Lanthanum-substituted bismuth titanate for use in non-volatile memories. *Nature* **1999**, *401*, 682–684. [[CrossRef](#)]
25. Scott, J.F.; Ross, F.M.; Paz de Araujo, C.A.; Scott, M.C.; Huffman, M. Structure and Device Characteristics of $\text{SrBi}_2\text{Ta}_2\text{O}_9$ -Based Nonvolatile Random-Access Memories. *MRS Bull.* **1996**, *21*, 33–39. [[CrossRef](#)]
26. Shet, T.; Bhimireddi, R.; Varma, K.B.R. Grain size-dependent dielectric, piezoelectric and ferroelectric properties of $\text{Sr}_2\text{Bi}_4\text{Ti}_5\text{O}_{18}$ ceramics. *J. Mater. Sci.* **2016**, *51*, 9253–9266. [[CrossRef](#)]
27. Yang, B.B.; Guo, M.Y.; Song, D.P.; Tang, X.W.; Wei, R.H.; Hu, L.; Yang, J.; Song, W.H.; Dai, J.M.; Lou, X.J.; et al. $\text{Bi}_{3.25}\text{La}_{0.75}\text{Ti}_3\text{O}_{12}$ thin film capacitors for energy storage applications. *Appl. Phys. Lett.* **2017**, *111*, 183903. [[CrossRef](#)]

28. Pan, Z.B.; Wang, P.; Hou, X.; Yao, L.M.; Zhang, G.Z.; Wang, J.; Liu, J.J.; Shen, M.; Zhang, Y.J.; Jiang, S.L.; et al. Fatigue-Free Aurivillius Phase Ferroelectric Thin Films with Ultrahigh Energy Storage Performance. *Adv. Energy Mater.* **2020**, *10*, 2001536. [[CrossRef](#)]
29. Tomar, M.S.; Melgarejo, R.E.; Hidalgo, A.; Mazumder, S.B.; Katiyar, R.S. Structural and ferroelectric studies of $\text{Bi}_{3.44}\text{La}_{0.56}\text{Ti}_3\text{O}_{12}$ films. *Appl. Phys. Lett.* **2003**, *83*, 341. [[CrossRef](#)]
30. Do, D.; Kim, S.S.; Kim, J.W.; Lee, Y.I.; Bhalla, A.S. Orientation Dependence of Ferroelectric and Dielectric Properties in $\text{CaBi}_4\text{Ti}_4\text{O}_{15}$ Thin Films. *Integr. Ferroelectr.* **2009**, *105*, 99–106. [[CrossRef](#)]
31. Kato, K.; Suzuki, K.; Nishizawa, K.; Miki, T. Ferroelectric properties of alkoxy-derived $\text{CaBi}_4\text{Ti}_4\text{O}_{15}$ thin films on Pt-passivated Si. *Appl. Phys. Lett.* **2001**, *78*, 1119. [[CrossRef](#)]
32. Kato, K.; Fu, D.; Suzuki, K.; Tanaka, K.; Nishizawa, K.; Miki, T. Ferro- and piezoelectric properties of polar-axis-oriented $\text{CaBi}_4\text{Ti}_4\text{O}_{15}$ films. *Appl. Phys. Lett.* **2004**, *84*, 3771. [[CrossRef](#)]
33. Kato, K.; Tanaka, K.; Suzuki, K.; Kimura, T.; Nishizawa, K.; Miki, T. Impact of oxygen ambient on ferroelectric properties of polar-axis-oriented $\text{CaBi}_4\text{Ti}_4\text{O}_{15}$ films. *Appl. Phys. Lett.* **2005**, *86*, 112901. [[CrossRef](#)]
34. Kim, S.S.; Kim, W.-J. Electrical properties of sol-gel derived pyrochlore-type bismuth magnesium niobate $\text{Bi}_2(\text{Mg}_{1/3}\text{Nb}_{2/3})_2\text{O}_7$ thin films. *J. Cryst. Growth* **2005**, *281*, 432–439. [[CrossRef](#)]
35. Kim, S.S.; Park, M.H.; Chung, J.K.; Kim, W.-J. Structural study of a sol-gel derived pyrochlore $\text{Bi}_2\text{Ti}_2\text{O}_7$ using a Rietveld analysis method based on neutron scattering studies. *J. Appl. Phys.* **2009**, *105*, 061641. [[CrossRef](#)]
36. Cho, S.Y.; Choi, G.P.; Jeon, D.H.; Johnson, T.A.; Lee, M.K.; Lee, G.J.; Bu, S.D. Effects of excess Bi_2O_3 on grain orientation and electrical properties of $\text{CaBi}_4\text{Ti}_4\text{O}_{15}$ ceramics. *Curr. Appl. Phys.* **2015**, *15*, 1332–1336. [[CrossRef](#)]
37. kato, k.; Suzuki, k.; tanaka, k.; Fu, D.; Nishizawa, k.; Miki, T. Effect of amorphous TiO_2 buffer layer on the phase formation of $\text{CaBi}_4\text{Ti}_4\text{O}_{15}$ ferroelectric thin films. *Appl. Phys. A* **2005**, *81*, 861–864. [[CrossRef](#)]
38. Jiao, L.L.; Liu, Z.M.; Hu, G.D.; Cui, S.G.; Jin, Z.J.; Wang, Q.; Wu, W.B.; Yang, C.H. Low-Temperature Fabrication and Enhanced Ferro- and Piezoelectric Properties of $\text{Bi}_{3.7}\text{Nd}_{0.3}\text{Ti}_3\text{O}_{12}$ Films on Indium Tin Oxide/Glass Substrates. *J. Am. Ceram. Soc.* **2009**, *92*, 1556–1559. [[CrossRef](#)]
39. Zheng, X.J.; Yang, Z.Y.; Zhou, Y.C. Residual stresses in $\text{Pb}(\text{Zr}_{0.52}\text{Ti}_{0.48})\text{O}_3$ thin films deposited by metal organic decomposition. *Scr. Mater.* **2003**, *49*, 71–76. [[CrossRef](#)]
40. Hu, G.D. Orientation dependence of ferroelectric and piezoelectric properties of $\text{Bi}_{3.15}\text{Nd}_{0.85}\text{Ti}_3\text{O}_{12}$ thin films on Pt(100)/ TiO_2 /SiO₂/Si substrates. *J. Appl. Phys.* **2006**, *100*, 096109. [[CrossRef](#)]
41. Yan, J.; Hu, G.D.; Liu, Z.M.; Fan, S.H.; Zhou, Y.; Yang, C.H.; Wu, W.B. Enhanced ferroelectric properties of predominantly (100)-oriented $\text{CaBi}_4\text{Ti}_4\text{O}_{15}$ thin films on Pt/Ti/SiO₂/Si substrates. *J. Appl. Phys.* **2008**, *103*, 056109. [[CrossRef](#)]
42. Hu, G.L.; Ma, C.R.; Wei, W.Z.; Sun, X.; Lu, L.; Mi, S.B.; Liu, M.; Ma, B.H.; Wu, J.; Jia, C.L. Enhanced energy density with a wide thermal stability in epitaxial $\text{Pb}_{0.92}\text{La}_{0.08}\text{Zr}_{0.52}\text{Ti}_{0.48}\text{O}_3$ thin films. *Appl. Phys. Lett.* **2016**, *109*, 193904. [[CrossRef](#)]
43. Xu, F.; Trolrier-McKinstry, S.; Ren, W.; Xu, B.M.; Xie, Z.-L.; Hemker, K.J. Domain wall motion and its contribution to the dielectric and piezoelectric properties of lead zirconate titanate films. *J. Appl. Phys.* **2001**, *89*, 1336–1348. [[CrossRef](#)]
44. Cruz, J.P.D.L.; Joanni, E.; Vilarinho, P.M.; Kholkin, A.L. Thickness effect on the dielectric, ferroelectric, and piezoelectric properties of ferroelectric lead zirconate titanate thin films. *J. Appl. Phys.* **2010**, *108*, 114106. [[CrossRef](#)]
45. Weibull, W. A Statistical Distribution Function of Wide Applicability. *J. Appl. Mech.* **1951**, *73*, 293–297. [[CrossRef](#)]
46. Tunkasiri, T.; Rujijanagul, G. Dielectric Strength of Fine Grained Barium Titanate Ceramics. *J. Mater. Sci. Lett.* **1996**, *15*, 1767–1769. [[CrossRef](#)]
47. Waser, R. TrI4: The Role of Grain Boundaries in Conduction and Breakdown of Perovskite-Type Titanates. *Ferroelectrics* **1992**, *133*, 109–114. [[CrossRef](#)]
48. Frey, M.H.; Xu, Z.; Han, P.; Payne, D.A. The role of interfaces on an apparent grain size effect on the dielectric properties for ferroelectric barium titanate ceramics. *Ferroelectrics* **1998**, *206*, 337. [[CrossRef](#)]
49. Hoshina, T.; Furuta, T.; Kigoshi, Y.; Hatta, S.; Horiuchi, N.; Takeda, H.; Tsurumi, T. Size Effect of Nanograined BaTiO_3 Ceramics Fabricated by Aerosol Deposition Method. *Jpn. J. Appl. Phys.* **2010**, *49*, 09MC02. [[CrossRef](#)]
50. Deng, X.Y.; Wang, X.H.; Wen, H.; Chen, L.L.; Chen, L.; Li, L.T. Ferroelectric properties of nanocrystalline barium titanate ceramics. *Appl. Phys. Lett.* **2006**, *88*, 252905. [[CrossRef](#)]
51. Sarkar, S.; Jana, P.K.; Chaudhuri, B.K. Colossal internal barrier layer capacitance effect in polycrystalline copper (II) oxide. *Appl. Phys. Lett.* **2008**, *92*, 022905. [[CrossRef](#)]
52. Yang, C.H.; Feng, C.; Lv, P.P.; Qian, J.; Han, Y.J.; Lin, X.J.; Huang, S.F.; Cheng, X.; Cheng, Z.X. Coexistence of giant positive and large negative electrocaloric effects in lead-free ferroelectric thin film for continuous solid-state refrigeration. *Nano Energy* **2021**, *88*, 106222. [[CrossRef](#)]
53. Wang, X.Z.; Huan, Y.; Zhao, P.Y.; Liu, X.M.; Wei, T.; Zhang, Q.W.; Wang, X.H. Optimizing the grain size and grain boundary morphology of (K,Na) NbO_3 -based ceramics: Paving the way for ultrahigh energy storage capacitors. *J. Mater.* **2021**, *7*, 780–789. [[CrossRef](#)]
54. Chao, X.L.; Ren, X.D.; Zhang, X.S.; Peng, Z.H.; Wang, J.J.; Liang, P.F.; Wu, D.; Yang, Z.P. Excellent optical transparency of potassium-sodium niobate-based lead-free relaxor ceramics induced by fine grains. *J. Eur. Ceram. Soc.* **2019**, *39*, 3684–3692. [[CrossRef](#)]
55. Watson, J.; Castro, G. High-Temperature Electronics Pose Design and Reliability Challenges. *Analog Dialog*. **2012**, *46*, 1–9.

56. Johnson, R.W.; Evans, J.L.; Jacobsen, P.; Thompson, J.R.; Christopher, M. The Changing Automotive Environment: High-Temperature Electronics. *IEEE Trans. Electron. Packag. Manuf.* **2005**, *27*, 164–176. [[CrossRef](#)]
57. Li, Q.; Chen, L.; Gadinski, M.R.; Zhang, S.H.; Zhang, G.Z.; Li, H.U.; Iagodkine, E.; Haque, A.; Chen, L.-Q.; Jackson, T.N.; et al. Flexible high-temperature dielectric materials from polymer nanocomposites. *Nature* **2015**, *523*, 576–579. [[CrossRef](#)]
58. Yan, J.; Wang, Y.L.; Wang, C.M.; Ouyang, J. Boosting energy storage performance of low-temperature sputtered $\text{CaBi}_2\text{Nb}_2\text{O}_9$ thin film capacitors via rapid thermal annealing. *J. Adv. Ceram.* **2021**, *10*, 627–635. [[CrossRef](#)]
59. Yang, B.B.; Guo, M.Y.; Song, D.P.; Tang, X.W.; Wei, R.H.; Hu, L.; Yang, J.; Song, W.H.; Dai, J.M.; Lou, X.J.; et al. Energy storage properties in $\text{BaTiO}_3\text{-Bi}_{3.25}\text{La}_{0.75}\text{Ti}_3\text{O}_{12}$ thin films. *Appl. Phys. Lett.* **2018**, *113*, 183902. [[CrossRef](#)]
60. Tang, Z.; Chen, J.Y.; Yang, B.; Zhao, S.F. Energy storage performances regulated by layer selection engineering for doping in multi-layered perovskite relaxor ferroelectric films. *Appl. Phys. Lett.* **2019**, *114*, 163901. [[CrossRef](#)]